Soft kink valves

Kai Luo [a,b,1], Philipp Rothemund [a,c,d,1], George M. Whitesides [c,d,e], Zhigang Suo [a,d,*]

[a] *John A Paulson School of Engineering and Applied Sciences, Harvard University, 29 Oxford St, Cambridge, MA 02138, USA*
[b] *MOE Key Laboratory of Dynamics and Control of Flight Vehicle, School of Aerospace Engineering, Beijing Institute of Technology, Beijing 100081, China*
[c] *Department of Chemistry and Chemical Biology, Harvard University, 12 Oxford Street, Cambridge, MA 02138, USA*
[d] *Kavli Institute for Bionano Science and Technology, Harvard University, 29 Oxford Street, Cambridge, MA 02138, USA*
[e] *Wyss Institute of Biologically Inspired Engineering, 60 Oxford Street, Cambridge, MA 02138, USA*

ARTICLE INFO

ABSTRACT

Completely soft, autonomous fluidic robots require valves made of soft materials. Such a soft valve has been demonstrated recently to enable complex movements of soft robots using a single source of air of constant pressure. This paper studies the mechanics of the valve using a combination of experiments and calculations. The valve is made of an elastomeric tube, subject to axial compression. At critical compression, the tube snaps into a kink and blocks the flow of the air in the tube. At another critical compression, the tube snaps open the kink and lets the air flow in the tube. The instability functions as a digital, on-and-off valve, and this function is unaffected by inaccurate deformation of the ends of the tube. A kinked tube blocks fluid flow in the tube up to a certain pressure. Because the elastomer readily undergoes large and reversible deformation, the kink valve can close and open repeatedly without damage. We map out the functional characteristics of the kink valve—the kink-close compression, the kink-open compression, and the breakthrough pressure—in the design space of material and geometry. It is hoped that this study will stimulate further work to harness diverse elastic instabilities for functions needed in soft robots.

1. Introduction

Soft robots can perform tasks that are difficult for hard robots (Whitesides, 2018). Examples include handling fragile objects, gripping objects of unknown shapes, squeezing through narrow gaps, and operating near humans. Many soft robots are actuated using elastomeric fluidic channels. Inflated by a fluid (either gas or liquid), the channels bend, extend, contract, and twist (Ainla et al., 2017; Fujiwara et al., 2009; Gong et al., 2016; Mosadegh et al., 2014; Yang et al., 2016). Many functions of soft robots are integrated into their bodies, but not all. In particular, off-the-shelf valves are mostly made of hard materials (Polygerinos et al., 2017; Rus and Tolley, 2015). When they are integrated onto a robot, complete softness of the robot is sacrificed (Tolley et al., 2014). Controls are therefore usually placed outside of the robot, tethered with tubes (Gong et al., 2016; Shepherd et al., 2011). Efforts are underway to develop on-board flow control using soft materials. Some soft control systems use fluid pressures to deform fluidic channels and, thus, constrain fluid flow

---

* Corresponding author.

E-mail address: suo@seas.harvard.edu (Z. Suo).

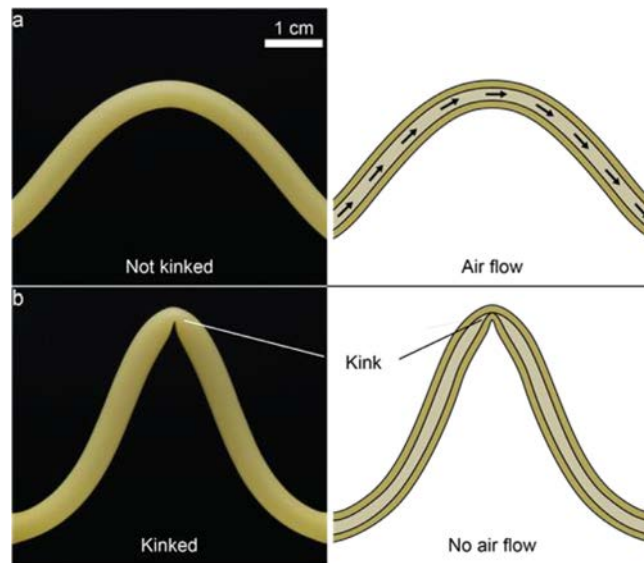[1] These authors contributed equally to this work.

Fig. 1. A kink valve made of an elastomeric tube subject to axial compression. The valve switches on and off the flow of air in the tube. (a) When the tube is not kinked, air flows through the tube, even when the tube bends. (b) When the tube forms a kink, the air flow stops. The photographs show a latex rubber tube (outer diameter $d_o = 0.476$ cm, inner diameter $d_i = 0.318$ cm).

(Mosadegh et al., 2010; Shepherd et al., 2013; Unger et al., 2000; Wehner et al., 2016). Others use the deformation of soft devices to influence the flow through embedded fluidic channels (Holmes et al., 2013).

We have recently described a soft kink valve (Rothemund et al., 2018). The valve consists of an elastomeric tube subject to axial compression. When the compression exceeds a critical value, the tube forms a kink, which blocks the fluid up to a certain pressure (Fig. 1, Video 1). The kink valve readily switches on and off a pneumatic soft robot (Video 2). When integrated in a feedback pneumatic circuit, the kink valve can use a single source of air, of constant pressure, to autonomously generate complex movements, such as grip and crawl. The kink valve has also enabled digital logic gates for complex control of soft robots (Preston et al., 2019). The kink valve has several useful attributes. (i) The tube snaps into a kink at one compression, and snaps open the kink at another compression. This instability makes an elastomer perform a digital function: an on-and-off valve. Because of the hysteresis of the instability, the function of the valve is not affected by small variations of the compression of the tube (e.g., due to viscoelasticity of a surrounding material to which the tube is connected). (ii) Because the elastomer readily undergoes large and reversible deformation, the kink valve can repeatedly close and open without damage (Rothemund et al., 2018). (iii) The kink forms by the deformation of the tube, which can be coupled with the deformation of a soft robot, enabling embedded feedback control to achieve complex movements of the robot. (iv) The functional characteristics of the valve—the compression for the onset of the kink, the compression for the removal of the kink, and the breakthrough pressure—depend on the geometry and the material of the tube, offering a large design space. (v) A tube matching the requirements of a specific application can be chosen from numerous existing off-the-shelf tubes, and does not have to be fabricated separately.

The working principle of the kink valve differs from that of a collapsible tube. A collapsible tube collapses, when the inner pressure falls below the outer pressure, which leads to a decrease in the cross-sectional area and, thus, to an increase in flow resistance. The giraffe, for example, controls the blood flow through its jugular vein based on this principle (Pedley et al., 1996). The mechanics of collapsible tubes and the influence of changes of the cross section on fluid-flow have been studied previously (Grotberg and Jensen, 2004; Pedley and Luo, 1998; Sisavath et al., 2001; Tavakol et al., 2017).

Kinks in tubes of hard materials (e.g., metals and plastics) have been extensively studied (Abramowicz and Jones, 1997; Alexander, 1960; Andrews et al., 1983; Corona and Kyriakides, 1988; Kecman, 1983). Brazier first showed that the cross section of a circular tube ovalizes when loaded beyond a critical bending moment (Brazier, 1927). The ovalization progresses with increasing bending load until the walls of the tube collapse with a local kink (Tanaka and Noguchi, 2006). The interaction between Euler buckling under axial compression and Brazier's instability in a thin, cylindrical tube has also been studied (Takano, 2013). Because hard materials cannot undergo large and reversible deformation, tubes of hard materials cannot function as kink valves.

Here we map out the functional characteristics of the kink valve in the design space of geometry and material. Even though a kink causes large deformation, most elastomers at such a level of deformation are still well represented by the neo-Hookean model, characterized by a single material parameter, the shear modulus. Consequently, different elastomers only affect the kink valve through the shear modulus, which scales the breakthrough pressure—the sealing capacity of the valve. This elementary consideration eliminates the need of further study of materials, so that the design space to be studied is spanned purely by the geometric parameters of the tube. Here we study the behavior of initially straight tubes. The

only geometric parameters are therefore the length, the inner diameter, the outer diameter. For a tube of a given geometry, we measure the functional characteristics of the kink valve: the compression at which the tube kinks and opens, the breakthrough pressure at which air starts to leak, and the pressure at which air leaks at a small constant rate. We use a finite element model to interpret the measured results. The kink valve harnesses an elastic instability of a soft material to enable a digital function. This paper aims to link roboticists and mechanicians. We hope that the results will aid roboticists in using the kink valve, and will also stimulate mechanicians to invent and study other elastic instabilities for useful functions.

2. Kink-close and kink-open compressions

To investigate the functional characteristics of the kink valve, we attached a latex rubber tube through barbed luer-lock fittings to a custom-made linear stage (Fig. 2a). The stage allowed controlled axial compression of the tube, but prohibited rotation and transverse motion of the ends. When the stage slides, the amount of compression is characterized by the ratio λ of the spacing between the two ends to the initial length of the tube. A kink blocks air of pressure p.

The tube is assumed to be incompressible and characterized by the shear modulus μ, outer diameter d_o, inner diameter d_i, and length L. We scale the pressure of the blocked air by the shear modulus of the tube, p/μ. The kink valve is a family of devices of two loading parameters, λ and p/μ, and of two-dimensional design space (d_o/d_i, L/d_i). We used latex rubber
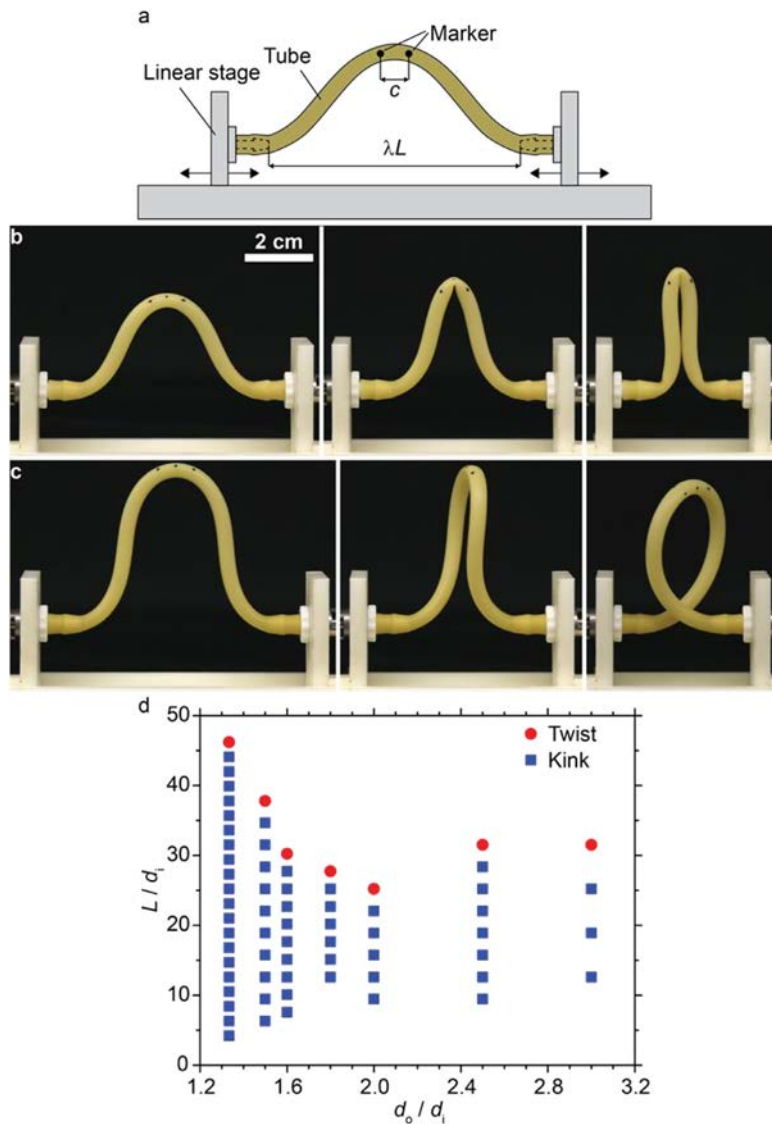

Fig. 2. Two modes of instability: kink and twist. (a) Linear stage for axial compression. (b) Under axial compression, a short tube forms a kink in the center, and then two kinks at the ends upon further compression. (c) A long tube does not kink, but twists. (d) Transition from kink to twist plotted in the design space (d_o/d_i, L/d_i).
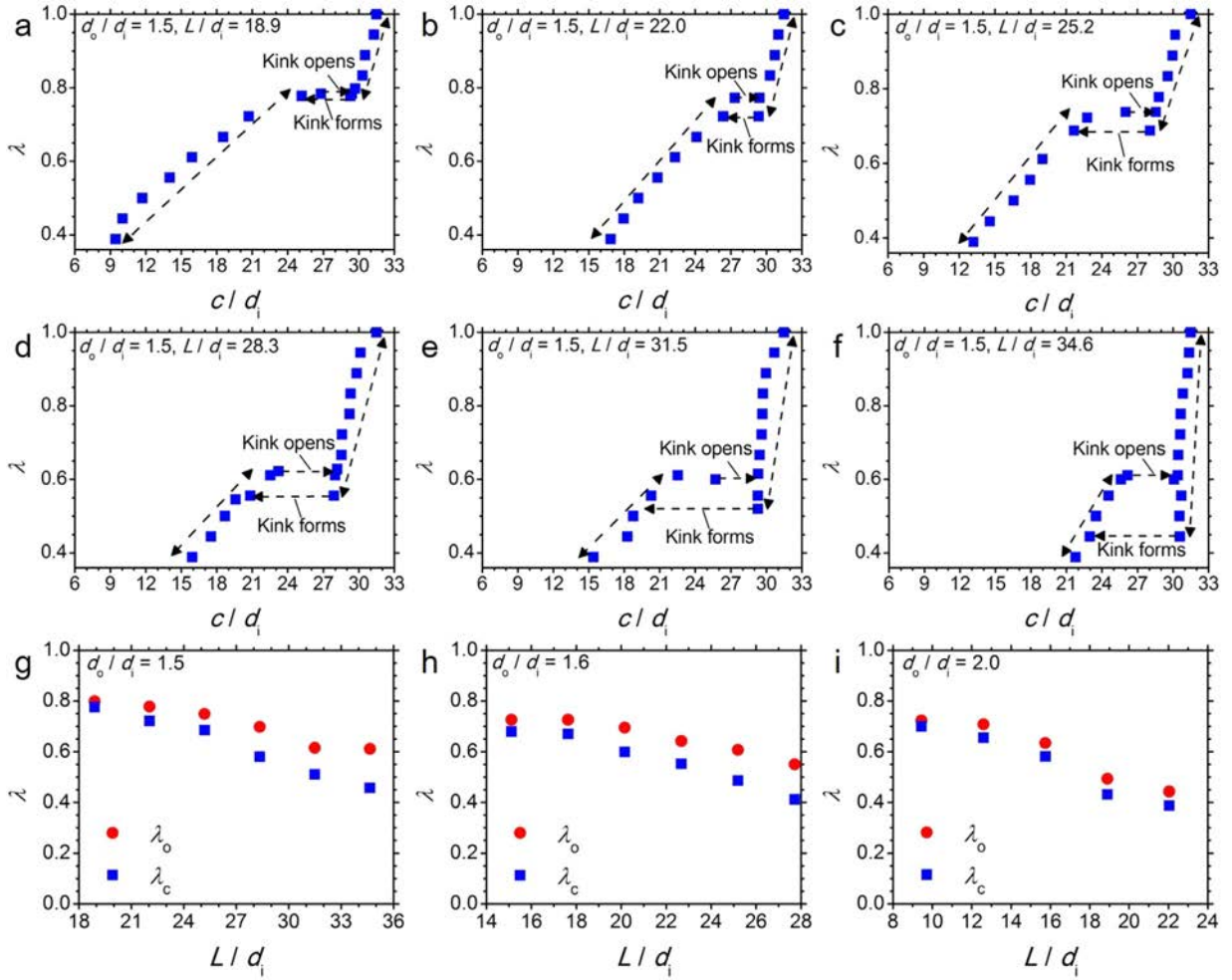
Fig. 3. (a–f) Experimentally determined bifurcation diagrams of six tubes of various combinations of d_o/d_i and L/d_i. The kink forms and opens at different compressions. A unidirectional arrow indicates the direction of snap into a kink or snap open a kink. A bidirectional arrow indicates smooth and reversible deformation, with or without kink. (g–i) The kink-close compression λ_c and the kink-open compression λ_o plotted as functions of the two design parameters, d_o/d_i and L/d_i.

tubes of three sizes: $d_o = 0.476$ cm and $d_i = 0.318$ cm (McMaster Carr 5234K241), $d_o = 0.635$ cm and $d_i = 0.397$ cm (McMaster Carr 5234K962), and $d_o = 0.635$ cm and $d_i = 0.318$ cm (McMaster Carr 5234K31). We characterize the elasticity of the tubes ourselves (Section 3).

At some small compressions all tubes underwent the Euler buckling (Fig. 2b, c). The smoothly bent tube did not block fluid flow. Upon further compression, we observed two additional modes of instability. A short tube rapidly snapped into a kink in its center (Fig. 2b). When the external walls of the tube touched, two more kinks formed at the ends, where the tube was connected to the linear stage. A long tube did not kink, but instead twisted (Fig. 2c). We measured the transition from kink to twist, and plotted the result in the design space (d_o/d_i, L/d_i) (Fig. 2d). Long tubes twisted, which did not block fluid flow. We therefore did not further consider twisted tubes.

We placed three markers spaced 0.5 cm in the center of a tube and measured the distance c between the outer markers as a function of λ (Fig. 3a–f). In such a bifurcation diagram, the distance c serves as a proxy for the state of the tube, and the compression λ is the loading parameter. During compression, the distance c between the markers decreased continuously until a critical amount of compression λ_c, at which the tube snapped into a kink. When the kink formed, c jumped to a smaller value. When the tube was compressed further, c again decreased continuously. When we reduced the axial compression after the kink formed, c increased continuously, until the kink snapped open. When the kink opened, c jumped to a larger value on the curve of the initial compression before formation of the kink.

The kink instability is hysteretic: the tube snap-close a kink at one compression λ_c, and snap-open the kink at another compression λ_o. The two critical compressions are functions of the two dimensionless geometric parameters:

$$\lambda_c = f_1 \left(\frac{d_o}{d_i}, \frac{L}{d_i} \right) \tag{1a}$$

$$\lambda_o = f_2 \left(\frac{d_o}{d_i}, \frac{L}{d_i} \right) \tag{1b}$$

We plot the measured two critical compressions as functions of the two design parameters d_o/d_i and L/d_i (Fig. 3g–i). The gap $\lambda_o - \lambda_c$ (the hysteresis of the instability) enlarges as L/d_i increases, but reduces as d_o/d_i increases. The size of the deformations that occur in a soft robot varies greatly, depending on the scale and the mode of deformation of the robot. The kink valve must be able to match these deformations without losing function. The dependence of the kink-close compression and kink-open compression on the two design parameters L/d_i, and d_o/d_i allows the flexibility to match the critical compressions, at which the valve switches, and the hysteresis between the two states to the deformation required by a specific application.

3. Material characterization

To proceed further, we need to characterize the elasticity of the material. Consider a piece of the elastomer undergoing a homogeneous deformation. Subject to no force, the elastomer is a rectangular block of edges L_1, L_2, L_3 (Fig. 4a). When the faces of the block are subjected to forces F_1, F_2, F_3, the elastomer deforms into another rectangular block of edges l_1, l_2, l_3 (Fig. 4b). Define the stretches by

$$\gamma_1 = \frac{l_1}{L_1}, \quad \gamma_2 = \frac{l_2}{L_2}, \quad \gamma_3 = \frac{l_3}{L_3}. \tag{2}$$

Define the nominal stresses by

$$s_1 = \frac{F_1}{L_2 L_3}, \quad s_2 = \frac{F_2}{L_3 L_1}, \quad s_3 = \frac{F_3}{L_1 L_2}. \tag{3}$$

The elastomer is taken to be incompressible, so that $L_1 L_2 L_3 = l_1 l_2 l_3$ and $\gamma_1 \gamma_2 \gamma_3 = 1$. Let W be the Helmholtz function per unit volume of the elastomer. The elastomer is taken to be hyperelastic—that is, when the elastomer deforms under the isothermal condition, the change in the Helmholtz function equals the work done by the applied forces: $L_1 L_2 L_3 \delta W = F_1 \delta l_1 + F_2 \delta l_2 + F_3 \delta l_3$. Thus,

$$\delta W = s_1 \delta \gamma_1 + s_2 \delta \gamma_2 + s_3 \delta \gamma_3. \tag{4}$$

The elastomer is further taken to be neo-Hookean, so that the Helmholtz function is (Treloar, 1975)

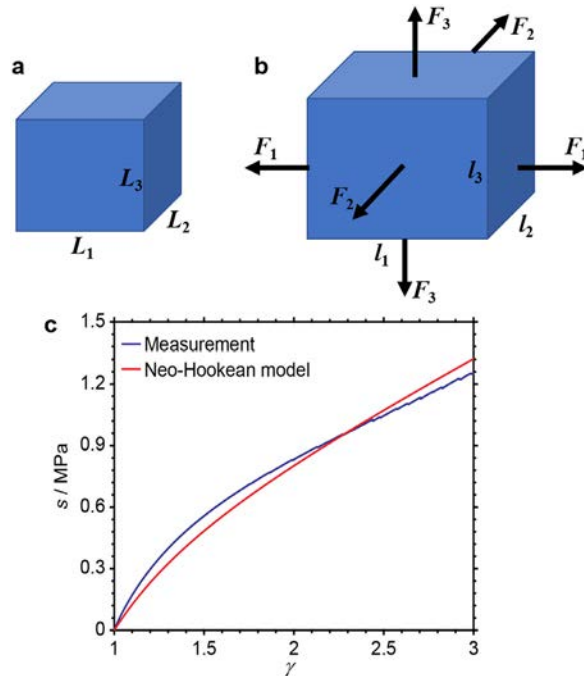$$W = \frac{\mu}{2} \left(\gamma_1^2 + \gamma_2^2 + \gamma_3^2 - 3 \right). \tag{5}$$

Fig. 4. Elastic deformation of an elastomer. (a) A rectangular block of the elastomer subject to no force. (b) The block deforms under forces. (c) The nominal stress s as a function of the axial stretch γ for the latex rubber tube during a uniaxial tensile test. The blue curve shows the experimental data. The red curve is a fit of the neo-Hookean material model to the data.

Inserting the condition of incompressibility, $\gamma_1\gamma_2\gamma_3 = 1$, the Helmholtz function is a function of two independent variables, $W = (\mu/2)(\gamma_1^2+\gamma_2^2+\gamma_1^{-2}\gamma_2^{-2} - 3)$, and $\delta\gamma_3 = -\gamma_1^{-2}\gamma_2^{-1}\delta\gamma_1 - \gamma_1^{-1}\gamma_2^{-2}\delta\gamma_2$, so that

$$\delta W = \left(s_1 - s_3\gamma_1^{-2}\gamma_2^{-1}\right)\delta\gamma_1 + \left(s_2 - s_3\gamma_1^{-1}\gamma_2^{-2}\right)\delta\gamma_2. \tag{6}$$

Consequently, the stress-stretch relations are

$$s_1 - s_3\gamma_1^{-2}\gamma_2^{-1} = \frac{\partial W(\gamma_1,\gamma_2)}{\partial\gamma_1} = \mu\left(\gamma_1 - \gamma_1^{-3}\gamma_2^{-2}\right), \tag{7a}$$

$$s_2 - s_3\gamma_1^{-1}\gamma_2^{-2} = \frac{\partial W(\gamma_1,\gamma_2)}{\partial\gamma_2} = \mu\left(\gamma_2 - \gamma_1^{-2}\gamma_2^{-3}\right). \tag{7b}$$

Under a state of uniaxial stress, $s_1 = s$, $s_2 = s_3 = 0$, $\gamma_1 = \gamma$, and $\gamma_2 = \gamma_3 = \gamma^{-1/2}$, the stress-stretch relation is $s = \mu(\gamma - \gamma^{-2})$. We fitted the neo-Hookean model to the stress-stretch curve measured from a latex rubber tube (Fig. 4c). The shear modulus obtained from this fit was $\mu = 550$ kPa.

4. Breakthrough pressure

When a tube kinks, the inner wall of the tube touches itself, blocking air flow through the tube. When the pressure of the blocked air is large enough, it can deform the tube to let the air break through. We define the pressure at which air starts to leak through the kink as the breakthrough pressure p_b. The breakthrough pressure characterizes the sealing capacity of the valve. The value of p_b can (for very soft materials) depend on adhesion between the walls of the tubing. For the material used here, we did not observe obvious adhesion between the walls of the tubing, so we assume that p_b only depends on the geometry and the stiffness of the tube, as well as on the axial compression:

$$\frac{p_b}{\mu} = f_3\left(\lambda, \frac{d_o}{d_i}, \frac{L}{d_i}\right). \tag{8}$$

To measure the breakthrough pressure p_b, we pressurized kinked tube with air from one side with a syringe pump (New Era Pump Systems Inc. NE-1000), and recorded the upstream pressure p_u using a pressure sensor (OMEGADYNE DPG409-100G-W, pressure range 0–100 psi, precision 0.001 bar) (Fig. 5a, b). The other side of the tube was connected to another pressure sensor (p_d) (Fig. 5a, b). When we pressurized the tube (flow rate $\dot{Q} = 1.0$ ml/min), p_u increased with the total air volume Q dispensed by the syringe pump (Fig. 5c). Initially, the downstream pressure on the other side of the kink (p_d) did not change with Q. When p_u reached a critical pressure, air started to leak through the seal increasing the pressure on the downstream side of the tube until the pressure on both sides of the tube were equal (Fig. 5c). We define the breakthrough pressure p_b to be value of p_u, when p_d reaches 1 kPa (Fig. 5c).

We measured the breakthrough pressure for tube of $d_o/d_i = 1.5$ as a function of the ratio L/d_i, and the compressive stretch λ (Fig. 5d). For λ near the kink-close compression λ_c, the breakthrough pressure was small, around 2.0 kPa (i.e., the sealing capacity was low). With decreasing λ, p_b increased. At the same compression λ, the breakthrough pressure was larger for a short tube than for a long tube. For a short tube, the length of the sections of the tube between the kink and the ends, at which rotation is blocked, is shorter and thus stiffer. For that reason, a larger force is exerted on the kink, which leads to a stronger seal. The pressures measured for this tube (up to 63.0 kPa) is large enough for many soft robotics applications (Rothemund et al., 2018; Whitesides, 2018). When compressed greatly, the tube of $L/d_i = 18.9$ kinked also at the ends near the luer-lock fittings. The extra kinks reduced the breakthrough pressure p_b (Fig. 5d).

5. Steady leak pressure

At the breakthrough pressure, air begins to leak through the kink. The rate of the leak $\dot{Q}$ at the breakthrough pressure is slow, and may, depending on the size of a soft robot, not affect the operation of the robot appreciably. To investigate the relationship between the upstream pressure and the rate of leak, we connected one end of the tube to a syringe pump and a pressure sensor, and connected the other end of the tube to a tube that ended in a container of water to allow air to flow freely (Fig. 6a, b). We visualized air flow through air bubbles in the water.

A method to characterize an elastic seal is to measure the upstream pressure p_u as a function of the quantity of the injected fluid Q at a constant rate of injection $\dot{Q}$ (Wang et al., 2017, 2015). We pressurized the tube with injection rates 0.5 ml/min $\leq \dot{Q} \leq 6$ ml/min. At all injections rates, the upstream pressure p_u increased with the total dispensed volume until it plateaued at a constant pressure, at which air leaked steadily through the kink at a rate $\dot{Q}$ equal to the injection rate of the syringe pump (Fig. 6c). We denoted the pressure of the plateau as the steady leaking pressure p_s. The lower $\dot{Q}$, the smaller was the p_s. At the lowest investigated injection rate $\dot{Q} = 0.5$ ml/min, p_s was twice the breakthrough pressure of this tube at the same stretch (Fig. 5c). The experiment demonstrates that the breakthrough pressure of the kink can be exceeded several fold before if a certain amount of leakage can be tolerated (e.g., the volume of the actuator used by Rothemund et al., was ~40 ml (Rothemund et al., 2018). At a rate of 0.5 ml/min it would take more than 1 h to leak all air out of the actuator.).
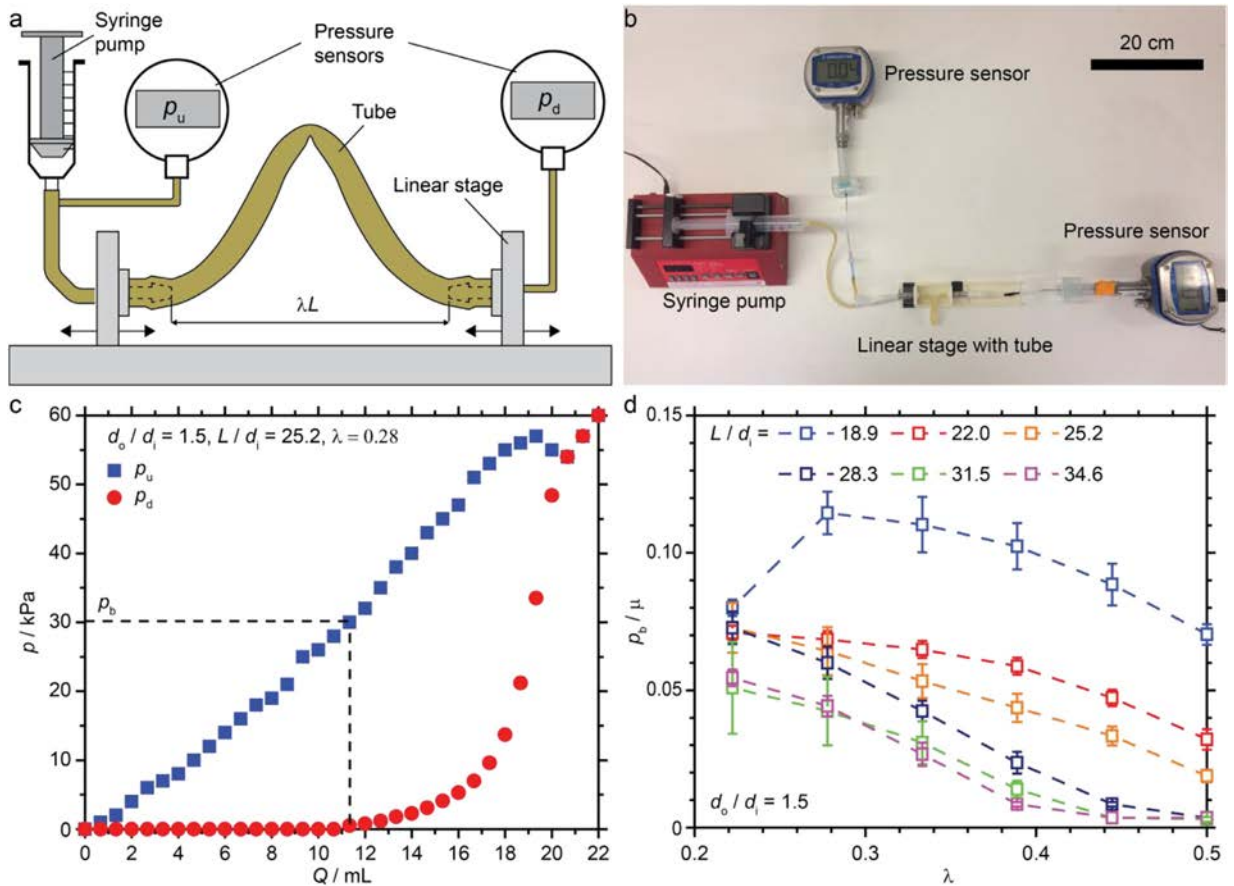
Fig. 5. The breakthrough pressure of a kinked tube. (a) Schematic of the experimental setup to measure the breakthrough pressure. (b) Photograph of the experimental setup. (c) Pressures at both sides of the tube as functions of the volume of the pumped air for a tube of $L/d_i = 25.2$ and $d_o/d_i = 1.5$, compressed at $\lambda = 0.28$. The breakthrough pressure p_b is defined as the upstream pressure when the downstream pressure reaches 1 kPa. (d) The breakthrough pressure as a function of L/d_i, and λ for tube with $d_o/d_i = 1.5$.

The steady leak pressure depends not only on the injection rate, but also on the geometry of the tube and the compressive stretch (Sisavath et al., 2001; Tavakol et al., 2017). We investigated the steady leaking pressure as a function of geometry of the tube, and the compressive stretch at the injection rate $\dot{Q} = 0.5$ ml/min (Fig. 6d). Like the breakthrough pressure (Fig. 5d), the steady leak pressure increased with the compression, and was larger for shorter tube than for longer tube at the same stretch (Fig. 6d). The steady leak pressures were larger than the breakthrough pressures.

6. Finite element simulation of the kink valve

We modeled the kink instability using the finite element software Abaqus/CAE 6.14-4 (Fig. 7). Because of the symmetry of the problem, we only modeled a quarter of the tube (Fig. 7a) using the appropriate symmetry boundary conditions. We used 8-node hexahedron elements (C3D8H) with a mesh size 0.2 mm and the isotropic neo-Hookean material model (C10 = 0.275 MPa, D1 = 0). We modeled the self-contact of the inner walls of the tube with the frictionless, hard surface-to-surface contact. To consider the possible contact between the two halves of the tube, we defined a frictionless, hard surface-to-surface contact between the outer wall of the tube, and the *xy* plane (Fig. 7a). To the ends of the tube, we applied compressive force in axial direction through a rigid body constraint. First, we performed the linear buckling analysis to obtain the Euler-buckling modes of the tube under axial compression. Then, we introduced the first buckling mode as a small initial geometrical imperfection from the initial geometry to facilitate Euler-buckling during the nonlinear simulation of the tubing under compression. We carried out the nonlinear simulation of the out-of-plane buckling and kinking of the tube using the Riks method.

We used in the simulation two nodes with the same distance from the center as the markers in the experiment (0.5 cm). Like in the experiments, the distance between the markers (*c*) initially decreased with the axial compression (λ) (Fig. 8a–f). At the onset of the kinking instability, the $\lambda - c/d_i$ curve exhibited a local minimum. While the kink formed, λ increased while *c* decreased. After the kink had formed, the distance between the markers decreased again monotonically with the
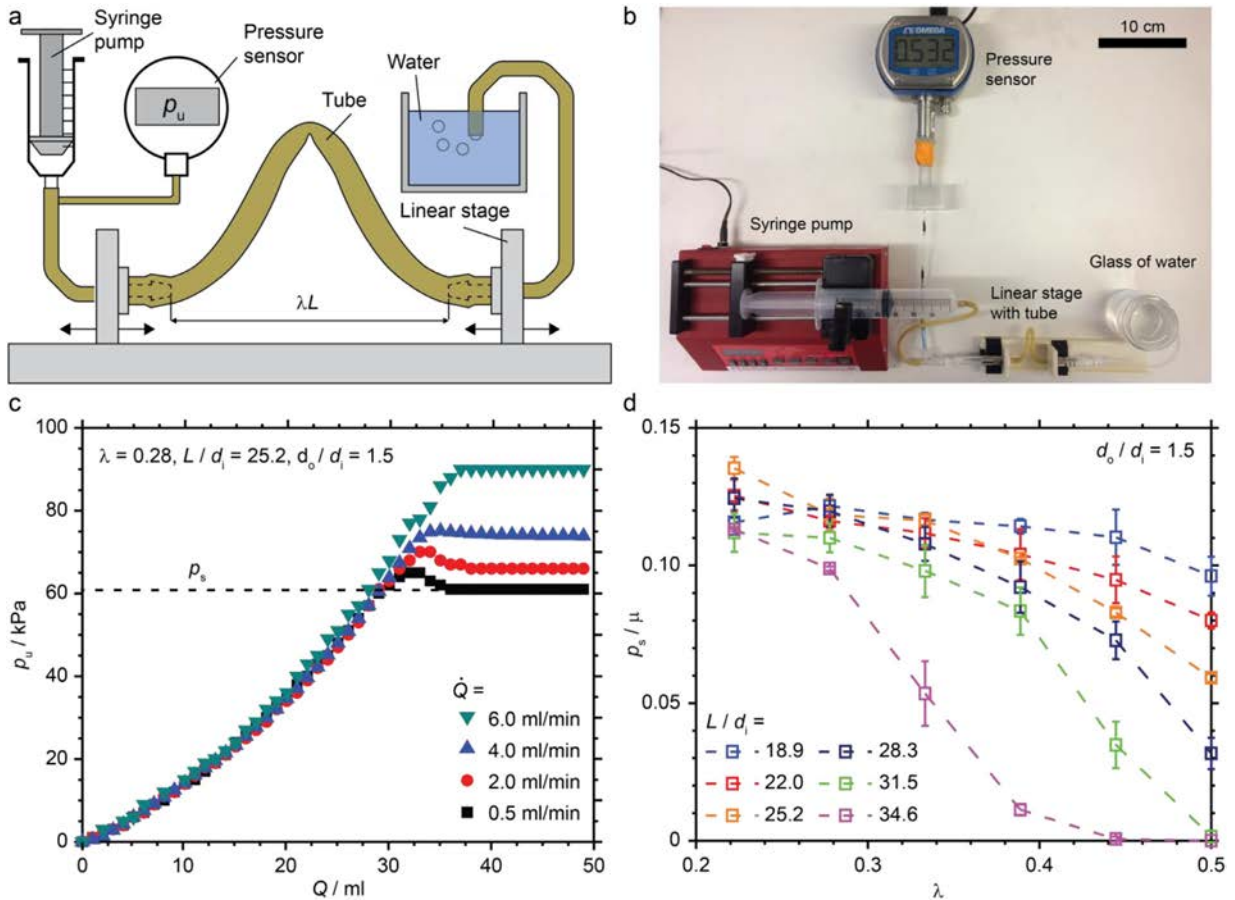
Fig. 6. Measurement of the steady leaking pressure. (a) Schematic of the experimental apparatus to measure the steady leaking pressure. (b) Photograph of the experimental apparatus. (c) The upstream pressure p_u as a function of total dispensed volume, and the injection rate for tube with $L/d_i = 25.2$, and $d_o/d_i = 1.5$ at $\lambda = 0.28$. The pressure at which p_u plateaus defines the steady leaking pressure p_s. (d) The steady leaking pressure as a function of λ and L/d_i for tube with $d_o/d_i = 1.5$.
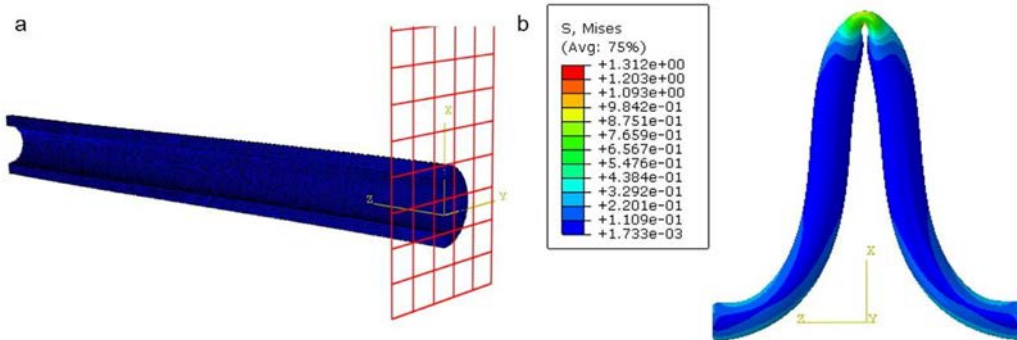

Fig. 7. Finite element model of tube. (a) A quarter-model was used to simulate kinking of the tube under axial compression. (b) Simulation of a kink ($L/d_i = 28.3$, $d_o/d_i = 1.5$, $\lambda = 0.33$, unit of the von Mises stress: MPa).

axial compression. During the formation of the kink, λ increased because the compressive force reduced (i.e., even though the distance between the markers decreases while the kink forms, the reduction in the axial force reduces the deformation away from the kink, leading to an overall increase distance between the ends of the tube.). In the experiment, this increase in λ was not observed, because λ was prescribed by the linear stage. Instead, the tube snapped into the kinked state, when the minimum of the curve was reached. Analogously, the maximum of the simulated λ – c/d_i corresponds to the critical condition, at which the kink opens. For $L/d_i = 18.9$ and $L/d_i = 22.0$ the simulation showed a fold instability at large
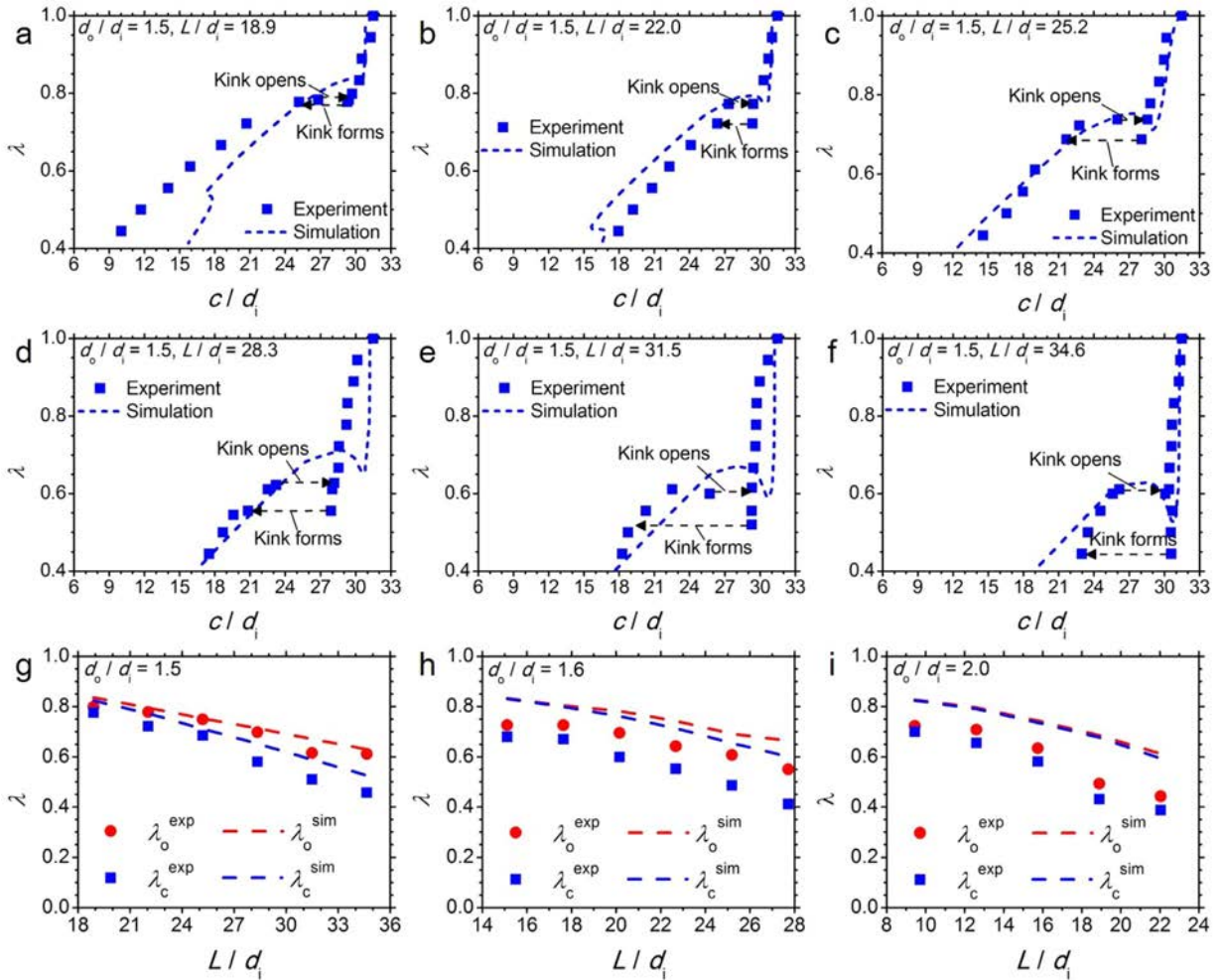
Fig. 8. Comparison of the experimental and simulated results of tubes under axial compression.

compression. This instability occurred when the tubes kinked near the ends where the displacements were prescribed. In the experiments, the tubes also formed kinks near the luer-lock connections at large compression, but they formed gradually.

We compared the results of the simulation with experimental data collected for tubes with different diameter ratios d_o/d_i and different ratios of length to inner diameter L/d_i (Fig. 8g–i). For $d_o/d_i = 1.5$, the experimental and the simulated critical stretches for formation and opening of the kink agree well (Fig. 8g). For larger d_o/d_i, the simulation captures the decrease of the size of the hysteresis between opening and closing of the kink well but overestimates the overall critical stretches. This discrepancy is likely due to neglecting the crease effect on the surface of the tube in the simulation.

7. Concluding remarks

We have studied kink valves using a combination of experiments and calculations. A kink forms and opens by snap at two levels of axial compression. The instability makes an elastomer perform a digital function: an on-and-off valve. This function is unaffected by the inaccurate deformation of the ends of the tube. The kink-close compression, the kink-open compression, and the breakthrough pressure can be tuned by material and geometry to match the design of a robot. The results presented here will aid the user of the kink valves. When the tube is embedded in a soft robot, the instability links fluid and elastomer in complex, surprising, and useful movements previously unimagined (Preston et al., 2019; Rothemund et al., 2018) . The kinked tube is an example of elastic instability. The variety of elastic instabilities is enormous; see two recent reviews (Holmes, 2019; Style et al., 2017). We hope that the present study will stimulate future work to harness these instabilities for diverse functions identified today, or imagined tomorrow.

Acknowledgments

Supplementary materials

Supplementary material associated with this article can be found, in the online version, at doi:10.1016/j.jmps.2019.07.008.

References

Abramowicz, W., Jones, N., 1997. Transition from initial global bending to progressive buckling of tubes loaded statically and dynamically. Int. J. Impact Eng. 19, 415–437.

Ainla, A., Verma, M.S., Yang, D., Whitesides, G.M., 2017. Soft, rotating pneumatic actuator. Soft Robot. 4, 297–304.

Alexander, J., 1960. An approximate analysis of the collapse of thin cylindrical shells under axial loading. Q. J. Mech. Appl. Math. 13, 10–15.

Andrews, K., England, G., Ghani, E., 1983. Classification of the axial collapse of cylindrical tubes under quasi-static loading. Int. J. Mech. Sci. 25 (, 9–10), 687–696.

Brazier, L., 1927. On the flexure of thin cylindrical shells and other "thin" sections. Proc. R. Soc. Lond. A 116, 104–114.

Corona, E., Kyriakides, S., 1988. On the collapse of inelastic tubes under combined bending and pressure. Int. J. Solids Struct. 24, 505–535.

Fujiwara, N., Sawano, S., Konishi, S., 2009. Linear expansion and contraction of paired pneumatic baloon bending actuators toward telescopic motion. In: MEMS 2009. IEEE 22nd International Conference on. IEEE, pp. 435–438.

Gong, X., Yang, K., Xie, J., Wang, Y., Kulkarni, P., Hobbs, A.S., Mazzeo, A.D., 2016. Rotary actuators based on pneumatically driven elastomeric structures. Adv. Mater. 28, 7533–7538.

Grotberg, J.B., Jensen, O.E., 2004. Biofluid mechanics in flexible tubes. Annu. Rev. Fluid Mech. 36, 121–147.

Holmes, D.P., 2019. Elasticity and stability of shape-shifting structures. Curr. Opin. Colloid Interface Sci. 40, 118–137.

Holmes, D.P., Tavakol, B., Froehlicher, G., Stone, H.A., 2013. Control and manipulation of microfluidic flow via elastic deformations. Soft Matter 9 (, 29), 7049–7053.

Kecman, D., 1983. Bending collapse of rectangular and square section tubes. Int. J. Mech. Sci. 25, 623–636.

Mosadegh, B., Kuo, C.-H., Tung, Y.-C., Torisawa, Y.-s., Bersano-Begey, T., Tavana, H., Takayama, S., 2010. Integrated elastomeric components for autonomous regulation of sequential and oscillatory flow switching in microfluidic devices. Nat. Phys. 6, 433.

Mosadegh, B., Polygerinos, P., Keplinger, C., Wennstedt, S., Shepherd, R.F., Gupta, U., Shim, J., Bertoldi, K., Walsh, C.J., Whitesides, G.M., 2014. Pneumatic networks for soft robotics that actuate rapidly. Adv. Funct. Mater. 24, 2163–2170.

Pedley, T., Luo, X., 1998. Modelling flow and oscillations in collapsible tubes. Theoret. Comput. Fluid Dyn. 10, 277–294.

Pedley, T.J., Brook, B.S., Seymour, R.S., 1996. Blood pressure and flow rate in the giraffe jugular vein. Philos. Trans. R Soc. Lond. B Biol. Sci. 351, 855–866.

Polygerinos, P., Correll, N., Morin, S.A., Mosadegh, B., Onal, C.D., Petersen, K., Cianchetti, M., Tolley, M.T., Shepherd, R.F., 2017. Soft robotics: review of fluid-driven intrinsically soft devices; manufacturing, sensing, control, and applications in human-robot interaction. Adv. Eng. Mater. 19 (, 12), 1700016.

Preston, D.J., Rothemund, P., Jiang, H.J., Nemitz, M.P., Rawson, J., Suo, Z., Whitesides, G.M., 2019. Digital logic for soft devices. Proc. Natl. Acad. Sci. U.S.A. 116, 7750–7759.

Rothemund, P., Ainla, A., Belding, L., Preston, D.J., Kurihara, S., Suo, Z., Whitesides, G.M., 2018. A soft, bistable valve for autonomous control of soft actuators. Sci. Robot. 3 eaar7986.

Rus, D., Tolley, M.T., 2015. Design, fabrication and control of soft robots. Nature 521, 467.

Shepherd, R.F., Ilievski, F., Choi, W., Morin, S.A., Stokes, A.A., Mazzeo, A.D., Chen, X., Wang, M., Whitesides, G.M., 2011. Multigait soft robot. Proc. Natl. Acad. Sci. U.S.A. 108, 20400–20403.

Shepherd, R.F., Stokes, A.A., Freake, J., Barber, J., Snyder, P.W., Mazzeo, A.D., Cademartiri, L., Morin, S.A., Whitesides, G.M., 2013. Using explosions to power a soft robot. Angew. Chem. Int. Ed. 52, 2892–2896.

Sisavath, S., Jing, X., Zimmerman, R.W., 2001. Creeping flow through a pipe of varying radius. Phys. Fluids 13, 2762–2772.

Style, R.W., Jagota, A., Hui, C.-Y., Dufresne, E.R., 2017. Elastocapillarity: surface tension and the mechanics of soft solids. Annu. Rev. Condensed Matter Phys. 8, 99–118.

Takano, A., 2013. Interaction between Euler buckling and Brazier instability. J. Solid Mech. Mater. Eng. 7, 92–101.

Tanaka, M., Noguchi, H., 2006. Brazier instability analysis by nonlinear finite element method. Theoret. Appl. Mech. Jpn. 55, 31–40.

Tavakol, B., Froehlicher, G., Holmes, D.P., Stone, H.A., 2017. Extended lubrication theory: improved estimates of flow in channels with variable geometry. Proc. Math. Phys. Eng. Sci. 473, 20170234.

Tolley, M.T., Shepherd, R.F., Mosadegh, B., Galloway, K.C., Wehner, M., Karpelson, M., Wood, R.J., Whitesides, G.M., 2014. A resilient, untethered soft robot. Soft Robot. 1, 213–223.

Treloar, L.R.G., 1975. The Physics of Rubber Elasticity. Oxford University Press, USA.

Unger, M.A., Chou, H.-P., Thorsen, T., Scherer, A., Quake, S.R., 2000. Monolithic microfabricated valves and pumps by multilayer soft lithography. Science 288, 113–116.

Wang, Z., Chen, C., Liu, Q., Lou, Y., Suo, Z., 2017. Extrusion, slide, and rupture of an elastomeric seal. J. Mech. Phys. Solids 99, 289–303.

Wang, Z., Liu, Q., Lou, Y., Jin, H., Suo, Z., 2015. Elastic leak for a better seal. J. Appl. Mech. 82.

Wehner, M., Truby, R.L., Fitzgerald, D.J., Mosadegh, B., Whitesides, G.M., Lewis, J.A., Wood, R.J., 2016. An integrated design and fabrication strategy for entirely soft, autonomous robots. Nature 536, 451.

Whitesides, G.M., 2018. Soft robotics. Angew. Chem. Int. Ed. 57, 4258–4273.

Yang, D., Verma, M.S., So, J.H., Mosadegh, B., Keplinger, C., Lee, B., Khashai, F., Lossner, E., Suo, Z., Whitesides, G.M., 2016. Buckling pneumatic linear actuators inspired by muscle. Adv. Mater. Technol. 1, 1600055.